Non-Abelian generalization of non-Hermitian quasicrystals: $\mathcal{PT}$-symmetry breaking, localization, entanglement, and topological transitions

Longwen Zhou[*]

College of Physics and Optoelectronic Engineering, Ocean University of China, Qingdao 266100, China

Non-Hermitian quasicrystal forms a unique class of matter with symmetry-breaking, localization and topological transitions induced by gain and loss or nonreciprocal effects. In this work, we introduce a non-Abelian generalization of non-Hermitian quasicrystal, in which the interplay between non-Hermitian effects and non-Abelian quasiperiodic potentials create mobility edges and rich transitions among extended, critical and localized phases. These generic features are demonstrated by investigating three non-Abelian variants of the non-Hermitian Aubry-André-Harper model. A unified characterization is given to their spectrum, localization, entanglement and topological properties. Our findings thus add new members to the family of non-Hermitian quasicrystal and uncover unique physics that can be triggered by non-Abelian effects in non-Hermitian systems.

I. INTRODUCTION

Quasicrystals represent a type of aperiodic system with correlated disorder. They could exhibit metal-insulator transitions at finite amounts of quasiperiodic modulations even in one spatial dimension [1–5]. In recent years, gain and loss or nonreciprocal effects have been added to quasiperiodic lattices, leading to the discovery of a wide varieties of non-Hermitian quasicrystals (NHQCs) [6–45]. In typical situations, an NHQC with $\mathcal{PT}$-symmetry could possess a $\mathcal{PT}$-breaking transition together with a localization transition with the change of its non-Hermitian control parameters. This non-Hermitian localization transition might be further accompanied by the quantized change of a spectral winding number of the system, endowing it with nontrivial topological features [9,10]. In the presence of long-range hoppings [12], sublattice structures [27], or time-periodic modulations [36], the extended and localized phases in an NHQC can also be separated by a critical phase with mobility edges, and reentrant localization transitions could be generated by non-Hermitian effects in these cases. Despite great theoretical efforts, phase transitions in NHQCs have also been observed experimentally in photonic settings [40,41], motivating further studies of their intriguing topological and transport properties.

In lattice models, the realization and implication of non-Abelian gauge fields have attracted continued interest in the quantum engineering of materials and artificial systems (see Refs. [46–53] for reviews). Recently, genuine non-Abelian conditions were considered in different types of Hofstadter-like models [54], where intriguing forms of butterfly fractal spectra, localization transitions and gapped or gapless topological phases were identified [55–68]. Among them, the interplay between non-Hermiticity and non-Abelian gauge potential has been found to be able to generate trivial, quantum spin Hall and metallic phases in superconducting circuits [63]. Metal-insulator transitions in quasiperiodic lattices with non-Abelian U(2) and SU(2) gauge fields were also explored in several studies [56,65]. However, much less is known about what happens when non-Hermitian and non-Abelian effects coexist in a quasicrystal. Specially, it is interesting to know whether the cooperation between non-Hermiticity and non-Abelian quasiperiodic potentials could generate unique phases and transitions that are absent in the Hermitian or Abelian counterparts of the underlying systems. The resolution of this issue is also of great experimental relevance due to the recent realizations of NHQCs by photonic quantum walks, where synthetic spin-$1/2$ degrees of freedom and SU(2) gauge structures could appear in the dynamics [40,41]. These settings thus provide natural platforms to detect the potential new features of non-Abelian NHQCs.

In this work, we explore the combined effects of non-Hermiticity and non-Abelian potentials in one-dimensional (1D) quasicrystals. Focusing on prototypical settings of non-Hermitian Aubry-André-Harper (NHAAH) models, we reveal that the presence of non-Abelian quasiperiodic superlattices could extend a critical point of non-Hermitian localization into a critical region, in which extended and localized eigenstates coexist and are separated by mobility edges. With the change of gain and loss or nonreciprocal hopping strengths, the system could further enter and leave this non-Abelian-effect-induced critical phase through two different localization transitions, which each of them being characterized by the quantized jump of a spectral topological winding number. These properties are expected to be generic for any 1D non-Abelian NHQCs. In Secs. II and III, we introduce our non-Abelian NHAAH models, discuss their non-Abelian conditions, analyze their $\mathcal{PT}$-symmetries and present our methods of investigating their eigenspectrum, inverse participation ratios (IPRs), entanglement spectrum (ES), entanglement entropy (EE), and topological invariants. In Sec. IV, we uncover the phases and transitions in our

*zhoulw13@u.nus.edu

three representative non-Abelian NHQC models with different types of non-Hermitian effects. The physical properties of all these models are found to be much richer than their Abelian or Hermitian counterparts. They also form prototypical setups for the theoretical and experimental study of other non-Abelian potentials in NHQCs. We summarize our results and discuss potential future studies in Sec. V.

II. MODEL

In this work, we focus on non-Abelian generalizations of the NHAAH model. The latter represents a typical system in the study of NHQC. The Hamiltonian of an Abelian NHAAH model can usually be defined as

$$H_0 = \sum_n [J_L c_n^\dagger c_{n+1} + J_R c_{n+1}^\dagger c_n + V \cos(2\pi\alpha n + i\gamma) c_n^\dagger c_n]. \quad (1)$$

Here $c_n^\dagger$ (c_n) is the creation (annihilation) operator of a particle on the lattice site n. J_L (J_R) represents the nearest-neighbor hopping amplitude of a particle from right to left (left to right) in the lattice. V is the amplitude of the superlattice onsite potential. $i\gamma$ represents an imaginary phase factor for $\gamma \in \mathbb{R} \setminus \{0\}$, which could introduce onsite gain and loss into the lattice. The system described by H_0 becomes a 1D quasicrystal once α is chosen to be an irrational number. When $J_L = J_R = J$, it was shown that the system could undergo a $\mathcal{PT}$ transition, a localization transition and a topological transition all at once under the periodic boundary condition (PBC) if $e^{|\gamma_c|} = |2J/V|$ [10]. When $|\gamma| < |\gamma_c|$, all the eigenstates of H_0 are spatially extended with real eigenvalues, and the spectral topological winding number $w = 0$. When $|\gamma| > |\gamma_c|$, all the eigenstates of H_0 are spatially localized with complex eigenvalues, and the spectral topological winding number $w = 1$. When $J_L \neq J_R^*$ and $\gamma = 0$, H_0 describes an NHQC with nonreciprocal hoppings. In this case, a $\mathcal{PT}$, localization and topological triple phase transition was also found in the system under the PBC [9]. Assuming $J_L = Je^{-\beta}$ and $J_R = Je^\beta$ ($\beta \in \mathbb{R}$), the transition point is determined by $e^{|\beta_c|} = |V/(2J)|$. When $|\beta| < |\beta_c|$, all the eigenstates are localized with real eigenvalues, and the spectral topological winding number $w = 0$. When $|\beta| > |\beta_c|$, all the eigenstates are extended with complex eigenvalues, and the spectral topological winding number $w = 1$. Such a triple phase transition was recently observed in nonunitary quantum walks [40]. It is not hard to see that these two Abelian NHAAH models are dual with each other under the PBC. Up to the rescaling of some system parameters, one of them can be mapped to the other under discrete Fourier transformations [9,10]. Meanwhile, no critical phases with mobility edges were found in these Abelian NHQCs.

We now introduce an SU(2) extension of H_0, which serves our purpose of studying non-Abelian NHQCs. Based on the necessary and sufficient condition of non-Abelian potential for Aubry-André-Harper (AAH) models [66], we define the Hamiltonian of our system as

$$H = \sum_n \big[J_L \mathbf{c}_n^\dagger \sigma_0 \mathbf{c}_{n+1} + J_R \mathbf{c}_{n+1}^\dagger \sigma_0 \mathbf{c}_n$$
$$+ V \mathbf{c}_n^\dagger \big(e^{-i\phi} \Theta_n + e^{i\phi} \Theta_n^{-1} \big) \mathbf{c}_n \big]. \quad (2)$$

TABLE I. Definitions of model parameters in Eqs. (2) and (3). $J \in \mathbb{R}$ is the uniform part of hopping amplitude. $\beta \in \mathbb{R}$ controls the asymmetry of hopping amplitude. $\gamma \in \mathbb{R}$ controls the non-Hermiticity of onsite potential. $n \in \mathbb{Z}$ represents the unit cell index. α belongs to $\mathbb{R} \setminus \mathbb{Q}$ for a quasicrystal. We set $\alpha = (\sqrt{5} - 1)/2$ in this work. Other irrational values of α will generate similar results.

Model	Hopping amplitude	Phase modulation
1	$J_L = J$, $\quad J_R = 0$	$\theta_n = 2\pi\alpha n$
2	$J_L = Je^{-\beta}$, $\quad J_R = Je^\beta$	$\theta_n = 2\pi\alpha n$
3	$J_L = J_R = J$	$\theta_n = 2\pi\alpha n + i\gamma$

Here, different from H_0, $\mathbf{c}_n^\dagger = (c_{n,\uparrow}^\dagger, c_{n,\downarrow}^\dagger)$ denotes a two-component creation operator. $c_{n,\sigma}^\dagger$ creates a particle with spin σ ($=\uparrow, \downarrow$) on the lattice site n. σ_0 is the two by two identity matrix acting on the two spin degrees of freedom of the particle. $\phi \in [-\pi, \pi)$ represents an Abelian phase factor. V represents the amplitude of onsite potential. In this work, we choose

$$\Theta_n = e^{i\theta_n \sigma_y} e^{i\theta_n \sigma_z}, \quad (3)$$

where σ_y and σ_z are Pauli matrices. This choice could realize the effect of a genuine non-Abelian gauge potential if $[e^{i\theta_n \sigma_y} e^{i\theta_n \sigma_z}, e^{i\theta_n \sigma_z} e^{i\theta_n \sigma_y}] \neq 0$, which can be satisfied for $\theta_n \neq \{0, \pi/2, \pi, 3\pi/2\}$ [66]. For the models considered in this work, the choices of phase modulation θ_n are summarized in Table I. The non-Abelian condition is clearly met when the α in Table I takes irrational values, which is also required for us to realize a quasiperiodic potential. Note that the form of non-Abelian potential Θ_n is not unique, and other types of non-Abelian Hermitian AAH models exist in the literature [55,56,65]. Nevertheless, the models considered in this study should be sufficient to capture the general properties originated from the interplay between non-Hermitian and non-Abelian effects in 1D NHQCs.

To investigate the spectral and localization properties of non-Abelian NHQCs, we need to solve the eigenvalue equation $H|\psi\rangle = E|\psi\rangle$ for our models. We can first expand the state as $|\psi\rangle = \sum_n \mathbf{c}_n^\dagger \boldsymbol{\psi}_n |0\rangle$, with $\boldsymbol{\psi}_n = (\psi_{n,\uparrow}, \psi_{n,\downarrow})^T$ being a column vector for the two spin components of $|\psi\rangle$ on the site n. Inserting the expanded state into the eigenvalue equation, we arrive at

$$J_L \boldsymbol{\psi}_{n+1} + J_R \boldsymbol{\psi}_{n-1} + V \big(e^{-i\phi} \Theta_n + e^{i\phi} \Theta_n^{-1} \big) \boldsymbol{\psi}_n = E \boldsymbol{\psi}_n. \quad (4)$$

For a lattice with L sites, we denote the eigenenergies of H by $\{E_j | j = 1, 2, ..., 2L-1, 2L\}$. The right eigenvector of H with energy E_j is denoted by $|\psi_j\rangle = \sum_{n=1}^L \sum_{\sigma=\uparrow, \downarrow} \psi_{n,\sigma}^j |n, \sigma\rangle$, where $|n, \sigma\rangle = c_{n,\sigma}^\dagger |\emptyset\rangle$ and $|\emptyset\rangle$ represents the vacuum state. We assume that each right eigenvector $|\psi_j\rangle$ has been properly normalized, such that $\sum_{n,\sigma} |\psi_{n,\sigma}^j|^2 = 1$. For $J_L \neq J_R^*$ or $\Theta_n^{-1} \neq \Theta_n^\dagger$, H is non-Hermitian and its eigenvalues can be complex.

Models 1–3 defined through Eqs. (2), (3) and Table I could all possess real spectra due to their $\mathcal{PT}$ symmetries. This can be proved as follows. We first work out the term $e^{-i\phi}\Theta_n +$

$e^{i\phi}\Theta_n^{-1}$ in Eq. (4) by inserting Eq. (3) into it as

$$e^{-i\phi}e^{i\theta_n\sigma_y}e^{i\theta_n\sigma_z} + e^{i\phi}e^{-i\theta_n\sigma_z}e^{-i\theta_n\sigma_y}$$
$$= d_n^0\sigma_0 + d_n^x\sigma_x + d_n^y\sigma_y + d_n^z\sigma_z, \qquad (5)$$

where

$$d_n^0 = \cos\phi(\cos 2\theta_n + 1),$$
$$d_n^x = \sin\phi(\cos 2\theta_n - 1),$$
$$d_n^y = d_n^z = \sin\phi \sin 2\theta_n. \qquad (6)$$

The $\mathcal{P}$ operator leads to the spatial inversion $n \to -n$ in one dimension and the time-reversal $\mathcal{T} \equiv \mathcal{U}\mathcal{K}$, where $\mathcal{U}$ is a unitary operator and $\mathcal{K}$ takes the complex conjugation. For $\theta_n = 2\pi\alpha n + i\gamma$, the combined action of $\mathcal{P}$ and $\mathcal{K}$ leads to $(d_{-n}^0\sigma_0)^* = d_n^0\sigma_0$, $(d_{-n}^x\sigma_x)^* = d_n^x\sigma_x$, $(d_{-n}^y\sigma_y)^* = d_n^y\sigma_y$ and $(d_{-n}^z\sigma_z)^* = -d_n^z\sigma_z$. Since $d_n^y = d_n^z$ in Eq. (6), the term $e^{-i\phi}\Theta_n + e^{i\phi}\Theta_n^{-1}$ is invariant under the combined $\mathcal{PT}$ operation if $\mathcal{U}$ could execute a rotation following which $\sigma_y \to \sigma_z$ and $\sigma_z \to -\sigma_y$ in Eq. (5). This can be achieved by setting $\mathcal{U} = e^{-i\frac{\pi}{4}\sigma_x}$, so that $\mathcal{U}\sigma_y\mathcal{U}^\dagger = \sigma_z$ and $\mathcal{U}\sigma_z\mathcal{U}^\dagger = -\sigma_y$. Therefore, the Hamiltonian of Model 3 is symmetric under the combined operation of parity $\mathcal{P} : n \to -n$ and time-reversal $\mathcal{T} = e^{-i\frac{\pi}{4}\sigma_x}\mathcal{K}$, implying that it could have a real spectrum in its $\mathcal{PT}$-invariant phase. To see that Models 1 and 2 also share the same $\mathcal{PT}$-symmetry with Model 3, we take the PBC in Eq. (4) and perform the Fourier transformation for $\boldsymbol{\psi}_n$ from position to momentum spaces as

$$\boldsymbol{\psi}_n = \frac{1}{\sqrt{L}} \sum_{\ell=1}^{L} \boldsymbol{\varphi}_\ell e^{-i2\pi\alpha\ell n}. \qquad (7)$$

The eigenvalue equation for the first two models are then transformed to

$$\Lambda_\ell\boldsymbol{\varphi}_\ell + \Xi\boldsymbol{\varphi}_{\ell+2} + \Xi^\dagger\boldsymbol{\varphi}_{\ell-2} = E\boldsymbol{\varphi}_\ell, \qquad (8)$$

where

$$\Lambda_\ell = (J_L e^{-i2\pi\alpha\ell} + J_R e^{i2\pi\alpha\ell} + V\cos\phi)\sigma_0 - V\sin\phi\sigma_x,$$
$$\Xi = \frac{V}{2}\cos\phi\sigma_0 + \frac{V}{2}\sin\phi\sigma_x + \frac{V}{2i}\sin\phi\sigma_y + \frac{V}{2i}\sin\phi\sigma_z. \qquad (9)$$

Under the combined actions of $\mathcal{P} : \ell \to -\ell$ and $\mathcal{T} = e^{-i\frac{\pi}{4}\sigma_x}\mathcal{K}$ in momentum space, we can directly see that $\mathcal{PT}\Lambda_\ell = \Lambda_\ell\mathcal{PT}$ and $\mathcal{PT}\Xi^{(\dagger)} = \Xi^{(\dagger)}\mathcal{PT}$. The Hamiltonians of Models 1 and 2 in momentum representations are thus $\mathcal{PT}$-symmetric. Therefore, our Models 1-3 all have the $\mathcal{PT}$-symmetry. Their spectra are allowed to be real in the $\mathcal{PT}$-invariant regions. They may also undergo $\mathcal{PT}$-breaking transitions with the change of their non-Hermitian parameters. The models we introduced thus provide typical settings to explore $\mathcal{PT}$ transitions in non-Abelian NHQCs.

III. METHOD

In this section, we introduce relevant tools to characterize the spectrum, localization, entanglement and topological transitions in non-Abelian NHQCs. To capture the spectral

transition of H from real to complex (or vice versa), we introduce the following quantities:

$$E_{\mathrm{I}}^{\max} = \max_{j\in\{1,...,2L\}}(|\mathrm{Im}E_j|), \qquad (10)$$

$$E_{\mathrm{I}}^{\min} = \min_{j\in\{1,...,2L\}}(|\mathrm{Im}E_j|), \qquad (11)$$

$$\rho = \frac{1}{2L}\sum_{j=1}^{2L}\theta(|\mathrm{Im}E_j|), \qquad (12)$$

where the step function $\theta(x) = 1$ if $x > 0$ and $\theta(x) = 0$ if $x \leqslant 0$. For a given set of system parameters, we have $E_{\mathrm{I}}^{\max} = \rho = 0$ if all the eigenvalues of H are real. Conversely, if $E_{\mathrm{I}}^{\min} > 0$ and $\rho = 1$, all the eigenvalues of H are complex. When $0 < \rho < 1$, real and complex eigenvalues of H coexist in the spectrum. Therefore, we can use the functions in Eqs. (10)–(12) to characterize the global spectral properties of H and distinguish its different spectral regions, i.e., the entirely real, entirely complex, or a mixture of real and complex eigenvalues.

For the eigenstate $|\psi_j\rangle$ of H, we can define its IPRs and normalized participation ratios (NPRs) as $\mathrm{IPR}_j = \sum_{n,\sigma}|\psi_{n,\sigma}^j|^4$ and $\mathrm{NPR}_j = (2L \cdot \mathrm{IPR}_j)^{-1}$, where the factor 2 comes from the two spin degrees of freedom. At a given set of system parameters, the averages of IPRs and NPRs over all eigenstates are given by $\langle\mathrm{IPR}\rangle = \frac{1}{2L}\sum_{j=1}^{2L}\mathrm{IPR}_j$ and $\langle\mathrm{NPR}\rangle = \frac{1}{2L}\sum_{j=1}^{2L}\mathrm{NPR}_j$. Using these definitions, we can introduce the following quantities to characterize the localization nature of states in the system

$$\mathrm{IPR}^{\max} = \max_{j\in\{1,...,2L\}}(\mathrm{IPR}_j), \qquad (13)$$

$$\mathrm{IPR}^{\min} = \min_{j\in\{1,...,2L\}}(\mathrm{IPR}_j), \qquad (14)$$

$$\eta = \log_{10}(\langle\mathrm{IPR}\rangle\langle\mathrm{NPR}\rangle). \qquad (15)$$

For an extended (a localized) state, we have $\mathrm{IPR}_j \sim L^{-1}$ ($\mathrm{IPR}_j \sim \lambda_j$) and $\mathrm{NPR}_j \sim 1$ ($\mathrm{NPR}_j \sim L^{-1}$) in the limit $L \to \infty$, where λ_j is the L-independent localization length of state $|\psi_j\rangle$ [69]. Therefore, for a given set of system parameters, we have $\mathrm{IPR}^{\max} \to 0$ if all the eigenstates of H are extended (a metallic phase) and $\mathrm{IPR}^{\min} > 0$ if all the eigenstates of H are localized (an insulating phase) in the thermodynamic limit. The quantity η was first introduced to characterize critical phases, in which extended and localized eigenstates coexist and are separated in their energies by mobility edges [70]. Its applicability to NHQCs was further demonstrated in Ref. [35]. Due to the scaling properties of IPRs and NPRs with the system size, we would have $\eta \sim -\log_{10}(2L)$ for our non-Abelian NHQCs in the extended and localized phases, with $\eta \to -\infty$ in both cases in the limit $L \to \infty$. In the critical phase, $\langle\mathrm{IPR}\rangle\langle\mathrm{NPR}\rangle$ takes a finite value in the thermodynamic limit. η can thus be used to distinguish critical from metallic and insulating phases. We will use Eqs. (13)–(15) to characterize phases with different localization properties and explore localization-delocalization transitions in our non-Abelian NHQC models.

In Abelian NHQCs, it has been found that $\mathcal{PT}$-breaking and localization transitions are usually accompanied by topological transitions, which are depicted by quantized jumps of spectral topological winding numbers [9,10]. To check

whether similar results hold in non-Abelian NHQCs, we introduce the definition of spectral winding numbers under the PBC as

$$w_\ell = \int_0^{2\pi} \frac{d\vartheta}{2\pi i} \frac{\partial}{\partial \vartheta} \ln\{\det[H(\vartheta) - \mathcal{E}_\ell]\}, \quad \ell = 1, 2. \quad (16)$$

Depending on the explicit form of the model, ϑ may be interpreted as a synthetic flux going through the 1D ring formed by the PBC lattice, or a phase shift in the quasiperiodic superlattice potential. For Models 1 and 2 in Table I, the ϑ-dependence of H can be introduced by setting $J_L \rightarrow J_L e^{-i\vartheta/L}$ and $J_R \rightarrow J_R e^{i\vartheta/L}$. For Model 3, we can set $2\pi\alpha n + i\gamma \rightarrow 2\pi\alpha n + i\gamma + \vartheta/L$ in θ_n. The w_ℓ then counts the number of times the spectrum of $H(\vartheta)$ winds around a chosen base energy $\mathcal{E}_\ell$ on the complex plane when ϑ changes over a period from zero to 2π [35]. The base energy $\mathcal{E}_\ell$ is in general model-dependent. In our numerical calculations, we choose $\mathcal{E}_1$ ($\mathcal{E}_2$) to be the real part of energy of the first (last) eigenstate of H whose IPR deflects from zero with the change of system parameters. For Abelian NHAAH models with only extended and localized phases, we expect $\mathcal{E}_1 = \mathcal{E}_2$ and there is only a single winding number $w = w_1 = w_2$, which is the case in Refs. [9,10]. For a system that could also possess critical mobility edge phases, we expect a quantized jump in w_1 (w_2) when the system goes through a transition point between the extended and critical (critical and localized) phases. If the system only holds critical and extended (localized) phases, w_2 (w_1) will be ill-defined and we only expect a quantized change in w_1 (w_2) when the system passes through the boundary between the two phases. Therefore, the winding numbers (w_1, w_2) could provide us with sufficient information to describe the topological nature of localization transitions in non-Abelian NHQCs. Note in passing that in the Hermitian limit of H, $H(\vartheta)$ is also Hermitian with a real spectrum. (w_1, w_2) will then become identically zero, implying that the definition of winding number w_ℓ in Eq. (16) is unique to non-Hermitian systems. In the meantime, it is better to interpret the quantized jumps of (w_1, w_2) as invariants accompanying topological localization transitions in NHQCs, instead of treating them as topological numbers characterizing a whole extended, localized or critical mobility edge phase.

The ES and EE could provide us with important information about topological and quantum phase transitions from an information-theoretical perspective. In the context of Abelian NHQCs, localization transitions and mobility edges have been identified from the ES and EE [45]. In the absence of mobility edges, the EE was found to change discontinuously when the system goes through a localization-delocalization transition. In the critical phase, the EE of extended and localized states were found to show clear distinctions around the mobility edge [45]. For our non-Abelian NHQCs, we introduce the single-particle biorthogonal eigenvectors $|\psi_j^R\rangle$ and $|\psi_j^L\rangle$ of H as

$$H|\psi_j^R\rangle = E_j|\psi_j^R\rangle, \qquad H|\psi_j^L\rangle = E_j^*|\psi_j^L\rangle, \quad (17)$$

where $j = 1, ..., 2L$. The binormalization condition $\langle\psi_j^L|\psi_{j'}^R\rangle = \delta_{jj'}$ is satisfied and the completeness relation is expressed as $\sum_j |\psi_j^R\rangle\langle\psi_j^L| = 1$. Assuming that a collection of energy levels $\{E_m\} \subseteq \{E_j|j = 1, ..., 2L\}$ is populated each by a fermion, the many-particle wave function

of the system can be expressed as $|\Psi^R\rangle = \prod_m \psi_{Rm}^\dagger|\emptyset\rangle$ and $|\Psi^L\rangle = \prod_m \psi_{Lm}^\dagger|\emptyset\rangle$, where $\psi_{Rm}^\dagger$ ($\psi_{Lm}^\dagger$) creates a single-particle eigenstate $|\psi_m^R\rangle$ ($|\psi_m^L\rangle$) whose energy belongs to the set $\{E_m\}$. The many-particle density matrix of the system then takes the form $\rho = |\Psi^R\rangle\langle\Psi^L|$. To investigate the bipartite entanglement, we consider a partition of the system into two equal parts A and B in real space [71]. Tracing out the degrees of freedom belonging to the subsystem B, we obtain the reduced density matrix of subsystem A as $\rho_A = \text{Tr}_B\rho$, and the EE is given by $S = -\text{Tr}(\rho_A \ln \rho_A)$ [72]. For noninteracting fermions, ρ_A represents a Gaussian state and we can express it as $\rho_A = \frac{1}{Z}e^{-H_A}$, where Z is a normalization factor. The eigenspectrum $\{\xi_j|j = 1, ..., L\}$ of the entanglement Hamiltonian H_A forms the ES, which can be related to the eigenvalues $\{\zeta_j|j = 1, ..., L\}$ of the single-particle correlation matrix C as $\xi_j = \ln(\zeta_j^{-1} - 1)$ [73–80]. Here the matrix elements of C in real-space take the form of

$$C_{nn'} = \langle\Psi^L|c_n^\dagger c_{n'}|\Psi^R\rangle = \langle n'|P|n\rangle, \quad (18)$$

where $n, n' \in$ A. The projector $P = \sum_m |\psi_m^R\rangle\langle\psi_m^L|$, and the sum is taken over all occupied states. Due to the one-to-one correspondence between the spectra of C and H_A, we will also refer to the spectrum $\{\zeta_j|j = 1, ..., L\}$ of the correlation matrix C as the ES. Meanwhile, the EE can be expressed in terms of the correlation matrix spectrum as

$$S = -\sum_{j=1}^L [\zeta_j \ln \zeta_j + (1 - \zeta_j)\ln(1 - \zeta_j)]. \quad (19)$$

Therefore, both the ES and EE can be obtained from the spectrum of correlation matrix C restricted to the subsystem A. The tools introduced in this section allow us to investigate the physics of non-Abelian NHQCs from different and complementary perspectives. We expect these tools to be applicable to non-Abelian NHQC models beyond those considered in this work.

IV. RESULTS

In this section, we reveal the spectrum, localization, entanglement, and topological properties of non-Abelian NHQCs with the methods presented in the last section. We start with a relatively simple case, in which the non-Hermiticity is introduced by allowing particles to hop along only one direction of the lattice (Model 1 in Table I). We then consider two more general situations, in which the non-Hermitian effects are originated from asymmetric hoppings (Model 2 in Table I) and complex non-Abelian onsite potentials (Model 3 in Table I). Rich connections between different physical properties of non-Abelian NHQCs will be established for all the cases.

A. Unidirectional hopping

We start with a non-Hermitian generalization of non-Abelian AAH model, in which the hopping terms only allow particles to jump from right to left between neighboring sites. According to Eqs. (3), (4) and Table I, the eigenvalue equation of this Model 1 takes the form

$$J\boldsymbol{\psi}_{n+1} + V(e^{-i\phi}\Theta_n + e^{i\phi}\Theta_n^{-1})\boldsymbol{\psi}_n = E\boldsymbol{\psi}_n, \quad (20)$$
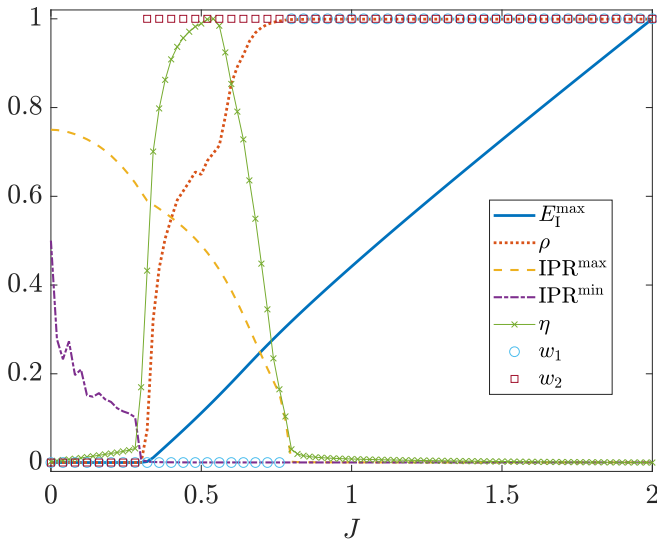
FIG. 1. Realness of the spectrum, IPRs and winding numbers of Model 1 versus the unidirectional hopping amplitude J [81]. Other system parameters are chosen as $V = 1$, $\phi = \pi/10$, and $\alpha = (\sqrt{5} - 1)/2$. The length of lattice is $L = 2584$.

where $\Theta_n = e^{i2\pi\alpha n\sigma_y} e^{i2\pi\alpha n\sigma_z}$. Referring to the last section, the system described by Eq. (20) possesses the $\mathcal{PT}$-symmetry, which implies that it could have real spectra under the PBC. This should happen when the unidirectional hopping amplitude J, which induces the non-Hermitian effect, is small compared with the other energy scales of the system. With the increase of J, we expect a transformation of the spectrum from real to complex when J goes beyond a critical value, which characterizes the $\mathcal{PT}$-breaking transition of the system. In the meantime, when $J \to 0$, the state profiles in the system are controlled by the non-Abelian onsite potential, and we expect all the eigenstates to be localized for an irrational α. In the opposite limit $J \to \infty$, the structures of states are dominated by the unidirectional hopping term. We expect all the eigenstates to be extended in this limit for a finite V. In between these two limits, there must be a delocalization transition for the eigenstates with the increase of J. In the Abelian case, such a transition happens at $J_c = V/2$ [18]. All the eigenstates change from localized to extended when J goes from below to above J_c, with their eigenvalues changing from real to complex. The localization and $\mathcal{PT}$-breaking transitions in the corresponding Abelian model thus go hand in hand with each other [18]. In Eq. (20), the non-Abelian potential introduces internal structures to each lattice site, which may transform the critical point J_c into a critical region $J \in (J_{c1}, J_{c2})$ with coexisting extended and localized eigenstates that are separated by mobility edges. The presence of such a critical phase in our system, which is due to the interplay between non-Hermitian and non-Abelian effects, will be revealed in the following calculations. Besides, the $\mathcal{PT}$ transition point shall be modified and only parts of eigenvalues in the spectrum may become complex after the transition first happens, as will be discussed below.

In Fig. 1, we present the maximal imaginary part of eigenenergies [Eq. (10)], the density of states with complex eigenvalues [Eq. (12)], the maximal [Eq. (13)] and minimal

[Eq. (14)] values of IPRs, the smoking gun function of critical phase [Eq. (15)], and the winding numbers [Eq. (16)] of Model 1 versus the hopping amplitude J for a typical case. We observe that when J is small ($J < J_{c1} \simeq 0.3$ in Fig. 1), all the eigenstates are indeed localized (IPR$^{min} > 0$) and their energies are real ($E_I^{max} = \rho = 0$), implying that the system is in a $\mathcal{PT}$-invariant localized phase in this region. When J is large enough ($J > J_{c2} \simeq 0.8$ in Fig. 1), all the eigenstates become extended (IPR$^{max} \to 0$) with complex eigenvalues ($\rho \to 1$), which means that the system is in a $\mathcal{PT}$-broken extended phase in the large-J region (we assume $V = 1$ as the unit of energy). With the increase of J from zero to a finite value J_{c1}, the system first undergoes a $\mathcal{PT}$-breaking transition signified by the emergence of complex eigenvalues (E_I^{max}, $\rho > 0$). This is accompanied by a delocalization transition through which certain eigenstates become extended (IPR$^{min} \to 0$). The $\mathcal{PT}$ and delocalization transitions at J_{c1} are correctly captured by the quantized jump of winding number w_2, which demonstrates their topological nature. Notably, not all eigenstates become extended following the first transition at J_{c1}, after which we still have localized states (IPR$^{max} > 0$). Therefore, a critical phase in which extended and localized eigenstates coexist appear in the intermediate region ($J_{c1} < J < J_{c2}$). States with real and complex eigenenergies are also coexistent in this phase ($0 < \rho < 1$). When J further increases up to J_{c2}, we encounter a second transition, through which all the eigenstates become extended and the spectrum is mostly complex. This transition is further characterized by the quantized jump of winding number w_1. Therefore, the collaboration between unidirectional hopping and non-Abelian quasiperiodic potential could create a localized phase with real spectrum, an extended phase with complex spectrum and a critical mobility edge phase with mixed spectrum, which are separated by a $\mathcal{PT}$-breaking transition and two localization transitions in Model 1. The absence of critical phases in the Abelian counterpart of Model 1 [18] confirms the importance of non-Abelian effects in our system.

To gain a deeper understanding about the mobility edges of the spectrum in the critical phase, we show the eigenenergies on the complex plane, the ES and the IPRs versus the real part of energy for three typical cases of Model 1 in Fig. 2. At each ReE, the ES is obtained by first filling all states whose real parts of energies are below ReE, and then following the procedure outlined in Sec. III. We see that when $J < J_{c1}$, all the eigenstates indeed have finite IPRs. The ES is pinned around $\zeta = 0$ and 1, suggesting vanishing contributions to the EE according to Eq. (19). This is expected, as each bulk state in this case is localized around a certain unit cell in either the subsystem A or B, not both. No signatures of mobility edges are observed in the spectrum. When $J > J_{c2}$, all the eigenstates are extended with vanishing IPRs, and a large portion of ES deviates from $\zeta = 0, 1$. The energy spectrum form two loops on the complex plane and no mobility edges are observed. The most interesting situation appears when $J = 0.5 \in (J_{c1}, J_{c2})$. From the IPRs in Fig. 2(h), we find localized states not only below a certain ReE but also at higher energies. The eigenenergies of these localized states are all real, as observed in Fig. 2(b). Therefore, the system could possess multiple mobility edges at different ReE in the critical phase. These mobility edges show clear signatures in the ES
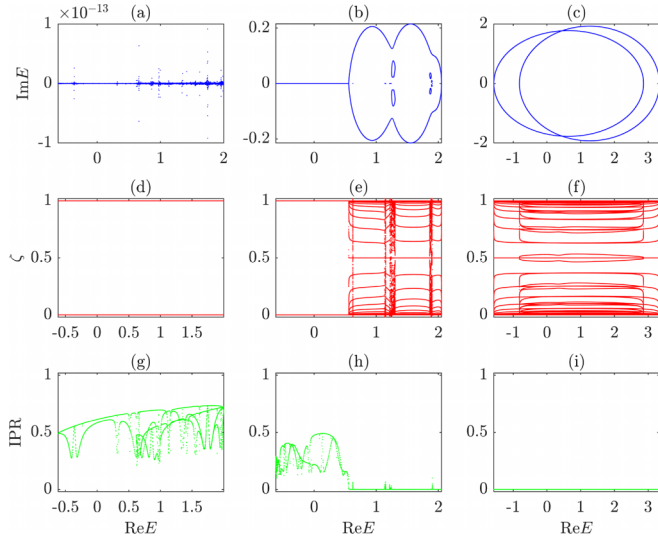
FIG. 2. Examples of eigenenergies, ES and IPRs for different phases of Model 1. The hopping amplitude is set to $J = 0.1$ for (a), (d), (g); $J = 0.5$ for (b), (e), (h); and $J = 2$ for (c), (f), (i). Other system parameters are chosen as $V = 1$, $\phi = \pi/10$ and $\alpha = (\sqrt{5}-1)/2$ for all panels. The length of lattice is $L = 2584$.

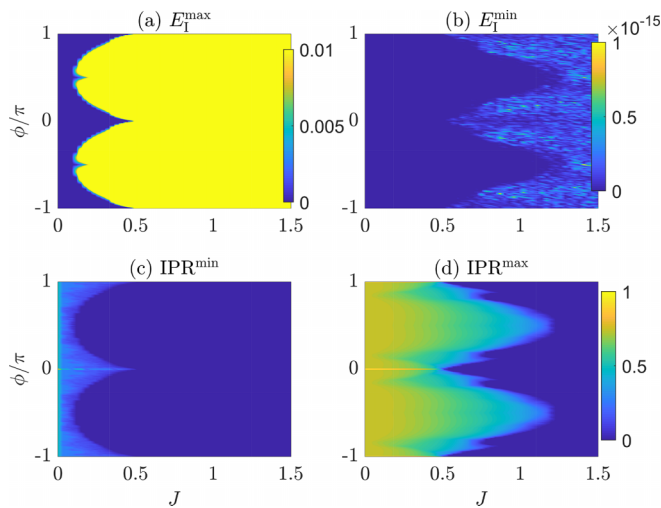FIG. 3. The maximum and minimum of the imaginary parts of eigenenergies and the IPRs versus the hopping amplitude J and the Abelian phase ϕ for Model 1. Other system parameters are $V = 1$ and $\alpha = (\sqrt{5}-1)/2$ for all panels. The length of lattice is $L = 610$. Panels (c) and (d) share the same color bar.
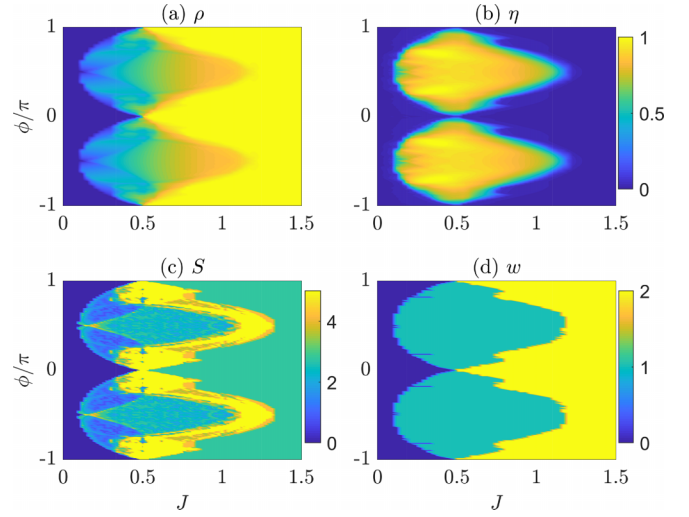

FIG. 4. The density of states with real energies, the smoking gun function of critical phase, the EE and the winding numbers versus the hopping amplitude J and the Abelian phase ϕ for Model 1 [81]. Other system parameters are $V = 1$ and $\alpha = (\sqrt{5}-1)/2$ for all panels. The length of lattice is $L = 610$. Panels (a) and (b) share the same color bar.

of Fig. 2(e). In Abelian NHQCs, signatures of mobility edges have been found in the ES [45]. Our results demonstrate that more complicated structures of mobility edges in non-Abelian NHQCs can also be identified from the distribution of ES at different energies.

To check the spectral and localization transitions in more general situations, we present the extreme values of ImE [Eqs. (10) and (11)] and IPRs [Eqs. (13) and (14)] versus the hopping amplitude J and the Abelian phase factor ϕ in Fig. 3. We find that the $\mathcal{PT}$-transition point could vary with ϕ in a nonmonotonic manner. Yet it is coincident with the

boundary between extended and critical phases at every ϕ, as shown in Figs. 3(a) and 3(c). Similarly, when the minimal values of ImE start to deviate from zero, the last localized eigenstate with IPR$^{\max} > 0$ vanishes and all the states become extended, as shown in Figs. 3(b) and 3(d). Note in passing that at $\phi = 0, \pm\pi$, the system can be reduced to two equivalent copies of Abelian unidirectional AAH models. Each of them has only a single transition point at $J_c = V/2$ and holding no critical phases [18]. Therefore, the presence of extended, critical, localized phases and the transitions among them are robust to the variation of phase factor ϕ ($\neq 0, \pm\pi$) in our non-Abelian NHQC Model 1.

Finally, we establish the phase diagram of our Model 1 from the entanglement and topological perspectives. In Fig. 4, we show the density of states with complex eigenvalues [Eq. (12)], the smoking gun function of critical phase [Eq. (15)], the EE [Eq. (19)], and the phase diagram determined by the winding number [Eq. (16)] of Model 1. Compared with the results of IPRs in Fig. 3, we clearly see that $\rho \to 0$ in the $\mathcal{PT}$-invariant localized phase, $\rho \to 1$ in the $\mathcal{PT}$-broken extended phase, and $0 < \rho < 1$ in the critical mobility edge phase highlighted by the η in Fig. 4(b). The EE is obtained by filling all the eigenstates with real energies at each given (J, ϕ) and following the steps in Sec. III. In Fig. 4(c), the EE is found to vanish throughout the localized phase, fluctuating in the critical phase while keeping a constant value $S \simeq 4 \ln 2$ in the extended phase. It can thus be employed as a good entanglement-based character to distinguish different phases in non-Abelian NHQCs. In Fig. 4(d), the blue, green, and yellow regions refer to the localized, critical, and extended phases, respectively. The boundary between the blue (green) and green (yellow) regions is the boundary around which the winding number w_2 (w_1) takes a quantized jump. These boundaries are well consistent with the phase boundaries identified from ρ, IPRs and S. Therefore, the winding

numbers (w_1, w_2) serve as topological order parameters to characterize the $\mathcal{PT}$ and localization transitions in our system. Putting together, we conclude that the cooperation between unidirectional hoppings and non-Abelian effects could indeed create many intriguing phases and transitions in a quasiperiodic lattice. In the following subsections, we will demonstrate that this physical picture holds for more general types of non-Hermitian effects and non-Abelian potentials.

B. Nonreciprocal hopping

We now consider a non-Abelian NHAAH model with nonreciprocal hopping amplitudes, which can be viewed as a generalized version of Model 1. According to Eqs. (4), (3) and Table I, the eigenvalue equation of Model 2 in position representation takes the form

$$Je^{-\beta}\boldsymbol{\psi}_{n+1} + Je^{\beta}\boldsymbol{\psi}_{n-1} + V\left(e^{-i\phi}\Theta_n + e^{i\phi}\Theta_n^{-1}\right)\boldsymbol{\psi}_n = E\boldsymbol{\psi}_n,$$
(21)

where $\Theta_n = e^{i2\pi\alpha n\sigma_y}e^{i2\pi\alpha n\sigma_z}$. The non-Hermitian effect is now introduced by an imaginary phase factor $i\beta$ accompanying the nearest-neighbor hopping amplitude. In the Abelian counterpart of this model, a $\mathcal{PT}$-transition together with a localization transition is predicted at $\beta_c = \ln[V/(2J)]$ for any irrational α, which is further characterized by the quantized jump of a spectral winding number from zero to one [9]. When $|\beta| < |\beta_c|$ ($|\beta| > |\beta_c|$), all the eigenstates of the Abelian NHQC are localized (extended) with a real (complex) spectrum under the PBC [9]. The non-Abelian Model 2 also possesses the $\mathcal{PT}$ symmetry, albeit different from its Abelian cousin in its explicit form as discussed in Sec. II. Therefore, we expect the system to reside in a localized (an extended) phase with real (complex) spectrum in the limit $\beta \to 0$ ($\beta \to \infty$) for any irrational α assuming $|J| \ll |V|$. $\mathcal{PT}$-breaking and localization transitions should happen at some finite values of β between these two limits. Furthermore, the non-Abelian potential may also help to expand the Abelian transition point β_c to a critical region $\beta \in (\beta_{c1}, \beta_{c2})$, in which extended and localized eigenstates coexist. This is similar to the situation encountered in Model 1. The presence of such a critical mobility edge phase and its properties in the non-Abelian NHQC Model 2 will be uncovered in the following discussions.

In Fig. 5, we present the maximal imaginary parts of eigenenergies [Eq. (10)], the density of states with complex eigenvalues [Eq. (12)], the maximal [Eq. (13)] and minimal [Eq. (14)] values of IPRs, the smoking gun function of critical phases [Eq. (15)], and the winding numbers [Eq. (16)] of Model 2 versus the nonreciprocal hopping parameter β for a typical case. From the IPR$^{\text{min}}$ and IPR$^{\text{max}}$, we identify two transition points at $\beta_{c1} \simeq 0.5$ and $\beta_{c2} \simeq 2.0$. When $\beta < \beta_{c1}$, all the eigenstates are localized (IPR$^{\text{min}} > 0$) and the spectrum is real (E_I^{max}, $\rho = 0$). The system thus resides in a $\mathcal{PT}$-invariant localized phase in this small-β region. When $\beta > \beta_{c2}$, all the eigenstates are extended (IPR$^{\text{max}} \to 0$) and the spectrum is complex. The system thus belongs to a $\mathcal{PT}$-broken extended phase in this large-β region. Interestingly, in the intermediate region with $\beta_{c1} < \beta < \beta_{c2}$, the spectrum is formed by comparable numbers of real and complex eigenvalues ($0 < \rho < 1$). Extended and localized eigenstates also
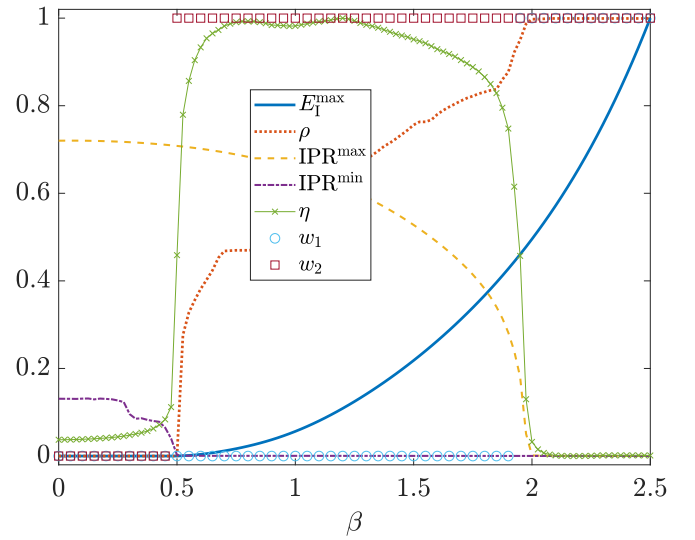

FIG. 5. Realness of the spectrum, IPRs, and winding numbers of Model 2 versus the nonreciprocal hopping modulation β [81]. Other system parameters are set as $J = 1$, $V = 6$, $\phi = \pi/2$, and $\alpha = (\sqrt{5} - 1)/2$. The length of lattice is $L = 2584$.

coexist in this region (IPR$^{\text{min}} \to 0$ yet IPR$^{\text{max}} > 0$), yielding a critical mobility edge phase as signaled by the function η. This critical phase is originated from the coexistence of non-Hermitian and non-Abelian potentials in our system. It is absent in the Abelian limit of our Model 2 [9]. Therefore, with the increase of β, the system first undergoes a $\mathcal{PT}$-breaking and delocalization transition at β_{c1}, which is also characterized by the quantized change of winding number w_2. When β further increases, we encounter a second delocalization transition at β_{c2}, which is accompanied by the quantized jump of another winding number w_1. The two separate transitions and the emerging critical phase are all unique to our non-Abelian NHQC model. The two transition points will merge at $\beta_c = \ln[V/(2J)] \simeq 1.1$ and the critical phase will disappear in the associated Abelian model [9]. These observations again demonstrate that non-Abelian potentials could induce richer phases and transition patterns in non-Hermitian quasiperiodic lattices.

To further decode the structure of mobility edges in the critical phase, we show the eigenenergies on the complex plane, the ES and the IPRs versus the real parts of energies for three typical cases of Model 2 in Fig. 6. At each given ReE, the ES is obtained by first filling all the eigenstates whose real parts of energies are below ReE, and then following the procedure outlined in Sec. II. We find that for the case with $\beta < \beta_{c1}$, all the eigenstates are indeed localized with finite IPRs and real energies. The ES is mostly pinned around $\zeta = 0, 1$ and no signatures of mobility edges are observed. A few ES values that deviate sufficiently away from $\zeta = 0, 1$ in Fig. 6(d) may originate from eigenmodes that are localized around the entanglement cuts between the subsystems A and B. In the case with $\beta > \beta_{c2}$, all the eigenmodes are found to be extended with vanishing IPRs. The spectrum form two loops on the complex plane in Fig. 6(c) and the eigenvalues are mostly complex. The ES contains notable portions that are away from
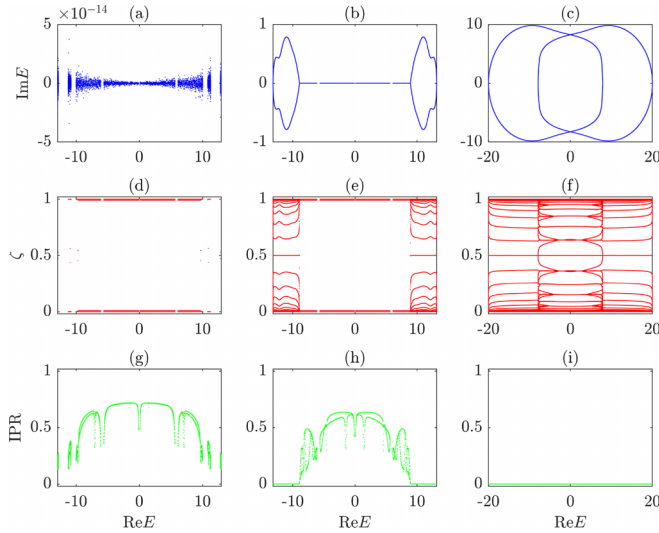
FIG. 6. Examples of eigenenergies, ES and IPRs for different phases of Model 2. The nonreciprocal hopping modulation is set to $\beta = 0.1$ for panels (a), (d), and (g); $\beta = 1.1$ for panels (b), (e), and (h); and $\beta = 2.5$ for panels (c), (f), and (i). Other system parameters are chosen as $J = 1$, $V = 6$, $\phi = \pi/2$, and $\alpha = (\sqrt{5} - 1)/2$ for all panels. The length of lattice is $L = 2584$.

$\zeta = 0, 1$ at every ReE, and no signatures of mobility edges are observed. In the intermediate case with $\beta = 1.1 \in (\beta_{c1}, \beta_{c2})$, we observe mobility edges at two different energies $E_{\pm}$ that are symmetric along the ReE axis, as shown in Figs. 6(b) and 6(h). Eigenstates whose Re$E \in (E_-, E_+)$ are localized with real energies, and otherwise extended with complex energies. These mobility edges can be clearly identified from the ES as shown in Fig. 6(e). Therefore, we can also use the ES as an information-based detector to find mobility edges in the spectrum and separate localized from delocalized states in our non-Abelian NHQC Model 2.

To check the $\mathcal{PT}$-breaking and localization transitions of our Model 2 in more general situations, we show the extreme values of ImE [Eqs. (10) and (11)] and IPRs [Eqs. (13) and (14)] versus the nonreciprocal hopping parameter β and the Abelian phase factor ϕ in Fig. 7. We observe that when the E_I^{max} starts to deviate from zero, the IPR^{min} goes to zero, which means that the $\mathcal{PT}$-breaking transition and the transition between localized and critical phases go hand-in-hand with each other in our system. This is true for every $\phi \in (-\pi, 0) \cup (0, \pi)$. At $\phi = 0, \pm\pi$, the critical phase vanishes due to the reducibility of our Model 2 to two identical copies of Abelian NHQCs [9], as mentioned before. Moreover, the boundary where E_I^{min} starts to deviate from zero is coincident with the boundary across which the IPR^{max} goes to zero, which means that most eigenstates have complex energies after the transition from critical to localized phases. This second phase boundary has a shape that can vary with ϕ in a nonmonotonous manner, and it merges with the first phase boundary at $\beta_c = \ln[J/(2V)]$ when $\phi = 0, \pm\pi$. Therefore, we conclude that our non-Abelian NHQC Model 2 indeed holds extended, critical and localized phases. It could further transform among them at different values of β and ϕ due to the interplay between nonreciprocal and non-Abelian effects.
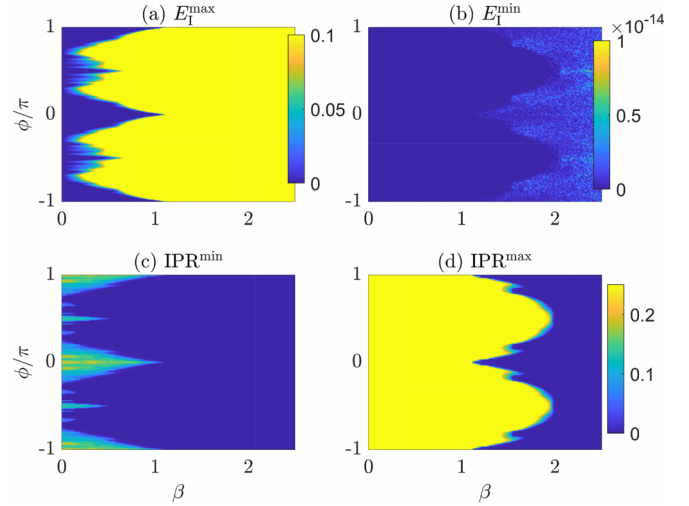

FIG. 7. The maximum and minimum of the imaginary parts of eigenenergies and the IPRs versus the nonreciprocal hopping modulation β and the Abelian phase ϕ for Model 2. Other system parameters are $J = 1$, $V = 6$ and $\alpha = (\sqrt{5} - 1)/2$ for all panels. The length of lattice is $L = 610$. Panels (c) and (d) share the same color bar.

We next build the phase diagram of our Model 2 from its entanglement and topological features. In Fig. 8, we show the density of states with complex eigenvalues [Eq. (12)], the smoking-gun function of critical phases [Eq. (15)], the EE [Eq. (19)], and the phase diagram decided by the winding numbers [Eq. (16)] of Model 2. Comparing Fig. 8(a) with the spectrum and IPRs in Fig. 7, we see that throughout the considered parameter regime, the density of states $\rho \to 0$ and $\rho \to 1$ in the real-spectrum localized phase and complex-spectrum extended phase, respectively. In the critical phase
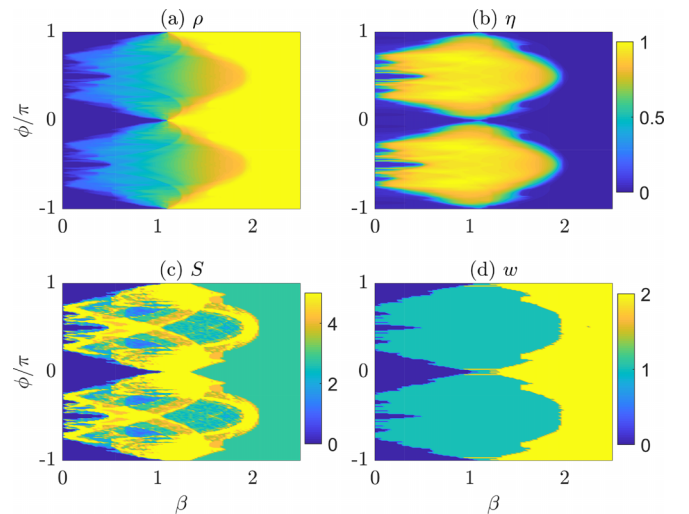

FIG. 8. The density of states with real energies, the smoking gun function of critical phase, the EE and the winding numbers versus the nonreciprocal hopping modulation β and the Abelian phase factor ϕ for Model 2 [81]. Other system parameters are $J = 1$, $V = 6$ and $\alpha = (\sqrt{5} - 1)/2$ for all panels. The length of lattice is $L = 610$. Panels (a) and (b) share the same color bar.

highlighted by η in Fig. 8(b), we have $0 < \rho < 1$, implying that real-energy localized states and complex-energy extended states coexist in this region. The EE in Fig. 8(c) is obtained by filling all the eigenstates with real energies at each (β, ϕ) and following the recipe discussed in Sec. III. We find the same EE $S = 0$ ($S \simeq 4 \ln 2$) in the $\mathcal{PT}$-invariant ($\mathcal{PT}$-broken) localized (extended) phase, and a fluctuating S in the critical mobility edge phase. Therefore, we can use the EE to clearly distinguish phases with different localization nature in our non-Abelian NHQC Model 2. Finally, by investigating the boundaries where the winding numbers w_2 and w_1 get quantized jumps, we obtain the borders of localized-to-critical and critical-to-extended phase transitions, which are well consistent with the boundaries predicted by the ρ, IPR$^{\max,\min}$ and S. The winding numbers $w_{1,2}$ can thus be adopted as topological order parameters to characterize the $\mathcal{PT}$ and localization transitions in our system. Figure 8(d) yields the phase diagram of Model 2, in which the blue, green, and yellow regions correspond to the localized, critical, and extended phases, respectively. To sum up, we find that the combined efforts of nonreciprocal hoppings and non-Abelian effects could also generate multiple intriguing phases with different localization properties and rich phase transitions in a quasiperiodic system. In the next subsection, we further explore the effects of a non-Abelian non-Hermitian onsite potential in generating these new phases.

C. Complex onsite potential

In the last example, we consider an NHAAH model with onsite gain and loss in a non-Abelian quasiperiodic potential. Following Eqs. (3), (4) and Table I, the eigenvalue equation of this Model 3 in the lattice representation reads

$$ J\boldsymbol{\psi}_{n+1} + J\boldsymbol{\psi}_{n-1} + V\left(e^{-i\phi}\Theta_n + e^{i\phi}\Theta_n^{-1}\right)\boldsymbol{\psi}_n = E\boldsymbol{\psi}_n, \quad (22) $$

where $\Theta_n = e^{i(2\pi\alpha n + i\gamma)\sigma_y} e^{i(2\pi\alpha n + i\gamma)\sigma_z}$. The hopping amplitude J is now symmetric and the non-Hermitian effect is introduced solely by the imaginary non-Abelian phase factor $i\gamma$. In the Abelian counterpart of the model, a $\mathcal{PT}$-breaking and localization transition can happen at $\gamma_c = \ln(2J/V)$ under the PBC for any irrational α, which is signified by the unit jump of a spectral winding number [10]. All the eigenstates are extended (localized) with real (complex) eigenvalues when $|\gamma| < |\gamma_c|$ ($|\gamma| > |\gamma_c|$), and no critical mobility edge phases are identified in the Abelian model [10]. Our Model 3 can be reduced to two equivalent copies of this Abelian model when we take $\phi = 0, \pm\pi$, with a critical point at $\gamma_c' = (1/2)\ln(2J/V)$. Since Model 3 also possesses the $\mathcal{PT}$-symmetry as discussed in Sec. II, we expect the system to exhibit an extended (a localized) phase with a real (complex) spectrum in the limit $\gamma \to 0$ ($\gamma \to \infty$) for any irrational α assuming $|J| \ll |V|$. $\mathcal{PT}$-breaking and localization transitions must happen between these two limits with the increase of γ. However, the non-Abelian potential may again extend the critical point γ_c' into a critical regime $\gamma \in (\gamma_{c1}, \gamma_{c2})$, in which extended and localized eigenstates can coexist and are separated by mobility edges. Eigenstates with real and complex energies may also survive together in this critical phase. In the following, we unveil the existence of such a critical phase and characterize the
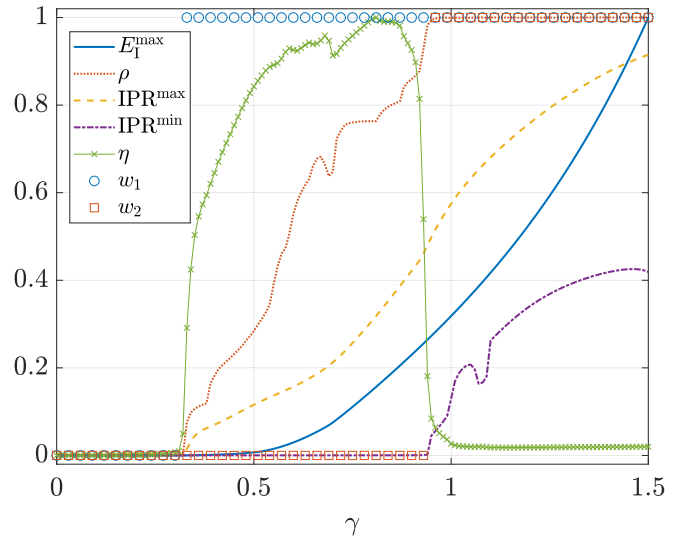

FIG. 9. Realness of the spectrum, IPRs and winding numbers of Model 3 versus the imaginary non-Abelian phase γ [81]. Other system parameters are set as $J = 1$, $V = 0.5$, $\phi = \pi/2$, and $\alpha = (\sqrt{5} - 1)/2$. The length of lattice is $L = 2584$.

transitions induced by non-Abelian non-Hermitian potentials between different phases in our Model 3.

In Fig. 9, we present the maximal ImE of all states [Eq. (10)], the density of states with complex energies [Eq. (12)], the maximal [Eq. (13)], and minimal [Eq. (14)] IPRs of all states, the smoking-gun function of critical phases [Eq. (15)] and the winding numbers [Eq. (16)] of Model 3 versus the imaginary non-Abelian phase shift γ for a typical example. From the IPRs, we can identify two localization transition points $\gamma_{c1} \simeq 0.31$ and $\gamma_{c2} \simeq 0.94$ with the deviations of IPR$^{\max}$ and IPR$^{\min}$ from zero during the increase of γ, respectively. γ_{c1} is also consistent with a $\mathcal{PT}$-breaking transition point, after which complex eigenvalues in energy start to emerge (with $E_I^{\max} > 0$). When $\gamma < \gamma_{c1}$, all the eigenstates are extended (IPR$^{\max} \to 0$) and carrying real energies ($E_I^{\max}, \rho = 0$). The system is thus in a $\mathcal{PT}$-invariant metallic phase in this region. When $\gamma > \gamma_{c2}$, all the eigenstates are localized (IPR$^{\min} > 0$) with most of them having complex energies ($\rho \to 1$). The system is thus in a $\mathcal{PT}$-broken insulating phase in this regime. When $\gamma \in (\gamma_{c1}, \gamma_{c2})$, extended (IPR$^{\min} \to 0$) and localized (IPR$^{\max} > 0$) eigenstates are found to coexist. Real and complex eigenvalues occupy comparable portions in the spectrum ($0 < \rho < 1$). This intermediate region thus corresponds to a critical mobility edge phase, as clearly highlighted by the function η in Fig. 9. Moreover, we observe a quantized jump of the winding number w_1 (w_2) when γ is swept across the transition point between extended (critical) and critical (localized) phases. The winding numbers $w_{1,2}$ can thus be used as topological order parameters to characterize the two different localization transitions in our non-Abelian NHQC Model 3. Note that these two transition points will merge into a single one at $\gamma_c' = \ln(4)/2 \simeq 0.69$ if $\phi = 0, \pm\pi$, for which our Model 3 is reduced to two Abelian copies of the model considered in Ref. [10]. The two localization transitions and the critical phase are thus all rooted in the presence of a non-Abelian non-Hermitian quasiperiodic
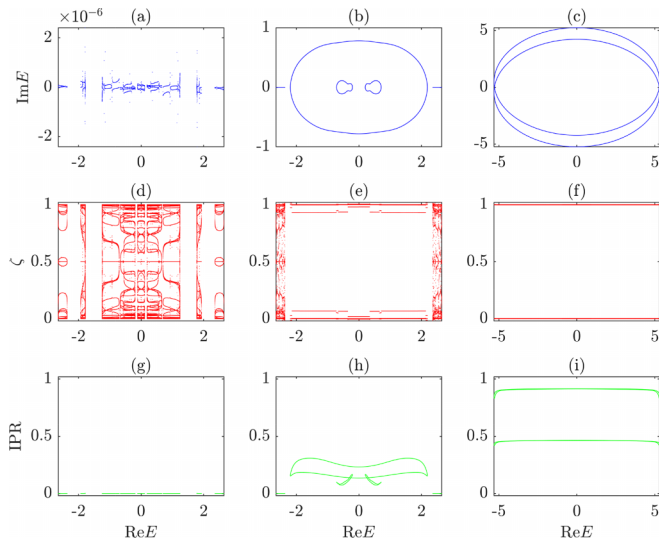
FIG. 10. Examples of the eigenenergies, ES and IPRs for different phases of Model 3. The imaginary phase is set to $\gamma = 0.1$ for panels (a), (d), and (g); $\gamma = 0.8$ for panels (b), (e), and (h); and $\gamma = 1.5$ for panels (c), (f), and (i). Other system parameters are chosen as $J = 1$, $V = 0.5$, $\phi = \pi/2$, and $\alpha = (\sqrt{5} - 1)/2$ for all panels. The length of lattice is $L = 2584$.

FIG. 11. The maximum and minimum of the imaginary parts of eigenenergies and the IPRs versus the imaginary phase γ and the hopping amplitude J for Model 3. Other system parameters are $V = 0.5$, $\phi = \pi/2$, and $\alpha = (\sqrt{5} - 1)/2$ for all panels. The length of lattice is $L = 610$. Panels (a) and (b) [(c) and (d)] share the same color bar.

potential in the system, through which richer patterns of phases and transitions beyond those in the Abelian counterpart of our Model 3 are generated [10].

To further analyze the structure of mobility edges induced by the non-Abelian potential, we present the spectrum on the complex plane, the ES and the IPRs versus the real part of energy for three typical cases of Model 3 in Fig. 10. At each given ReE, the ES is obtained by first filling all the eigenstates whose real parts of energies are below ReE, and then following the steps outlined in Sec. III. We find that for $\gamma > \gamma_{c2}$, all the eigenstates are indeed localized with finite IPRs, and the spectrum is constituted by two loops on the complex plane, as shown in Figs. 10(i) and 10(c). The ES in Fig. 10(f) is pinned around $\zeta = 0, 1$ for all ReE, which implies that the states below any energy are localized ether in the subsystem A or B of the lattice. The system in this case then resides in a localized phase and no signatures of mobility edges are observable. For $\gamma < \gamma_{c1}$, the spectrum is real and the IPRs of all states are vanishingly small, as shown in Figs. 10(a) and 10(g). From the ES in Fig. 10(d), we can see gaps in certain ranges of ReE. Meanwhile, sufficient parts of ES are away from $\zeta = 0, 1$ in other energy regions. In this case, the system belongs to a $\mathcal{PT}$-invariant extended phase with no signals of mobility edges. When $\gamma = 0.8 \in (\gamma_{c1}, \gamma_{c2})$, the spectrum contains both real and complex eigenvalues, as shown in Fig. 10(b). Referring to the IPRs in Fig. 10(h), we realize that the extended and localized eigenmodes separately have real and complex eigenvalues. Notably, these two types of states are split not only by mobility gaps but also by energy gaps at different ReE, which is distinct from the first two models considered in this section. In Fig. 10(e), we also observe gaps along the ReE axis. They separate states whose ES are close to $\zeta = 0, 1$ from the other states whose ES are distributed throughout the range $\zeta \in [0, 1]$. The energy and mobility gaps of Model 3 are thus
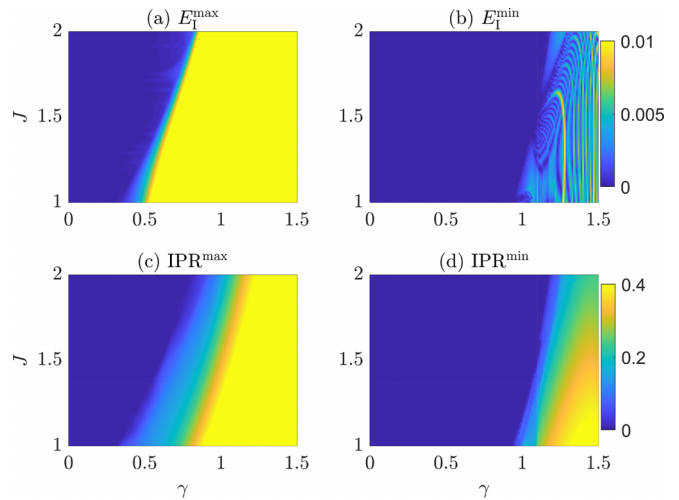
clearly identifiable from the ES. Therefore, we can apply the ES as a detector to seek for the energy and mobility gaps in the spectrum and distinguish the localized from delocalized states in our non-Abelian NHQC Model 3. The results presented in Figs. 2, 6, 10 also revealed the generality of ES as a tool to characterize the mobility edges in quasicrystals with different types of non-Hermitian and non-Abelian effects.

In Fig. 11, we report the extreme values of ImE [Eqs. (10) and (11)] and IPRs [Eqs. (13) and (14)] versus the imaginary non-Abelian phase γ and the hopping amplitude J for our Model 3. In Figs. 11(a) and 11(c), we observe that when the spectrum changes from real to complex across the $\mathcal{PT}$-transition boundary, the IPR$^{\text{max}}$ also increases from a vanishingly small value to a finite value at every given J. Therefore, the $\mathcal{PT}$-breaking transition of the spectrum happens together with the localization transition of the states between extended and critical phases. We have also verified this observation for different choices of the Abelian phase $\phi \in (-\pi, 0) \cup (0, \pi)$. Similarly, when the $E_{\text{I}}^{\text{min}}$ starts to deviate from zero in Fig. 11(b), all the eigenstates become localized through a second transition as shown in Fig. 11(d). The energies of eigenstates are mostly complex after the this transition from the critical to localized phases. Therefore, our non-Abelian NHQC Model 3 could also possess extended, critical and localized phases in a broad range of parameter domains. Moreover, the association between non-Hermitian and non-Abelian potentials enables interesting patterns of $\mathcal{PT}$-breaking and localization transitions among these phases. Together with the previous two models, our results here uncovered the rich physics that can be brought about by non-Abelian effects in NHQCs.

Finally, we present the the density of states with complex energies [Eq. (12)], the smoking-gun function of critical phases [Eq. (15)], the EE [Eq. (19)], and the phase diagram obtained from the winding numbers [Eq. (16)] of Model 3
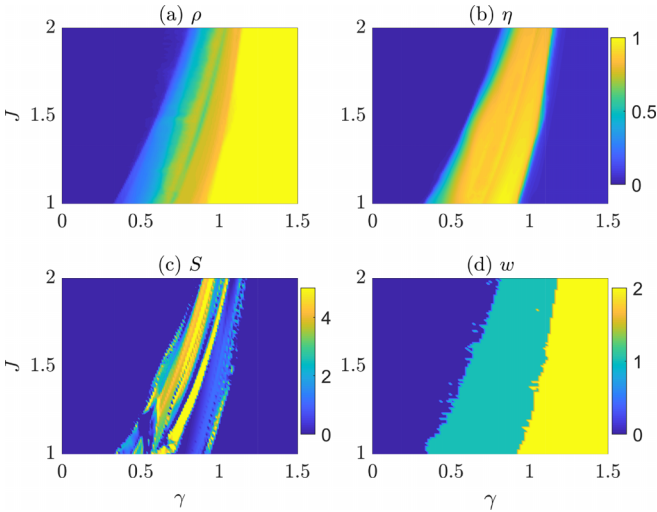
FIG. 12. The density of states with real energies, the smoking-gun function of critical phase, the EE and the winding numbers versus the imaginary phase γ and hopping amplitude J for Model 3 [81]. Other system parameters are $V = 0.5$, $\phi = \pi/2$, and $\alpha = (\sqrt{5} - 1)/2$ for all panels. The length of lattice is $L = 610$. Panels (a) and (b) share the same color bar.

versus γ and J in Fig. 12. We observe that in the regions with $\rho = 0$ and $\rho \rightarrow 1$ in Fig. 12(a), we also have IPR$^{\text{max}} \rightarrow 0$ and IPR$^{\text{min}} > 0$ in Figs. 11(c) and 11(d). These two regions thus correspond to a $\mathcal{PT}$-invariant metallic phase with real spectrum and a $\mathcal{PT}$-broken insulating phase with almost all eigenenergies being complex. The region in between represents a critical phase with sufficient amounts of coexisting real and complex eigenenergies in the spectrum ($0 < \rho < 1$). This intermediate phase and its two boundaries are clearly highlighted by the function η in Fig. 12(b). In Fig. 12(c), the EE is found to vanish ($S = 0$) both in the extended and localized phases. In the region of critical mobility edge phase, the EE fluctuates strongly, as also observed from the EE of the first two models. The phase diagram of Model 3 is shown in Fig. 12(d), where the blue, green, and yellow regions correspond to the extended, critical, and localized phases, respectively. The left and right boundaries are determined by the locations where w_1 and w_2 get quantized jumps, respectively. These boundaries are clearly coincident with the boundaries of the $\mathcal{PT}$-symmetry breaking and the two localization transitions identified from the results of ρ, IPR$^{\text{max,min}}$ and S. Therefore, both nonreciprocal hoppings and onsite gain/loss could collaborate with non-Abelian quasiperiodic potentials to yield different types of spectral transitions, topological localization transitions and critical mobility edge phases in NHQCs. Note in passing that the localization nature of eigenstates in our models may also be characterized by the energy-level statistics [82–87]. We give brief accounts of this issue in the Appendix.

V. CONCLUSION AND DISCUSSION

In this work, we found unique phases and transitions that could be induced by the interplay between non-Abelian potentials and different types of non-Hermitian effects in 1D

quasicrystals. For an NHQC with either nonreciprocal hoppings or onsite gain and loss, we revealed the emergence of a critical mobility edge phase when a non-Abelian quasiperiodic modulation was introduced. Such a critical phase could be separated from an extended phase and a localized phase by two topological localization transitions. One of the transitions could further accompany a real-to-complex spectral transition if the non-Abelian NHQC also possesses the $\mathcal{PT}$-symmetry. We expect these features to be generic for any 1D non-Abelian NHQC models. Our discoveries were further demonstrated by investigating the energy spectrum, inverse participation ratios, entanglement spectrum, entanglement entropy and spectral topological winding numbers for three prototypical non-Abelian generalizations of non-Hermitian AAH models, with each of them holding only a single $\mathcal{PT}$-breaking and localization transition in the absence of non-Abelian effects. In short, we will have no $\mathcal{PT}$-breaking transitions and topological spectral windings in the Hermitian limits, no critical phases in the Abelian limits, and no localization transitions in the crystal limits ($\alpha \in \mathbb{Q}$) of our models. The rich physics we found are thus originated from the interplay among three key factors, i.e., the non-Hermitian effect, the quasiperiodic modulation, and the non-Abelian potential. Our results thus enriched the study of NHQCs and uncovered the intriguing phases and transitions that could be brought about by non-Abelian effects.

The non-Abelian potentials considered in this work could be employed to induce critical phases in other 1D NHQCs. Qualitatively, the reason for the expansion of critical points in the Abelian limits of our models to critical phases in non-Abelian cases might be understood as follows. Let us consider Eqs. (4)–(6) in the paper. Without the $d_n^x \sigma_x$ and $d_n^y \sigma_y$ terms in Eq. (5), Eq. (4) can be decomposed into two spin polarized chains, which are described separately by

$$J_{\text{L}} \psi_{n+1,\uparrow} + J_{\text{R}} \psi_{n-1,\uparrow} + V \left(d_n^0 + d_n^z \right) \psi_{n,\uparrow} = E \psi_{n,\uparrow}, \quad (23)$$

$$J_{\text{L}} \psi_{n+1,\downarrow} + J_{\text{R}} \psi_{n-1,\downarrow} + V \left(d_n^0 - d_n^z \right) \psi_{n,\downarrow} = E \psi_{n,\downarrow}. \quad (24)$$

Referring to Eq. (6) of our three models, Eqs. (23) and (24) describe two Abelian quasicrystals with the same critical point between extended and localized phases. There are no critical phases with mobility edges in these two decoupled chains. When the interchain coupling terms $d_n^x \sigma_x$ and $d_n^y \sigma_y$ in Eq. (5) are switched on, the system in Eq. (4) becomes genuine non-Abelian. Moreover, the terms $d_n^x \sigma_x + d_n^y \sigma_y$ may induce an overlap between the extended band of the spin-$\uparrow$ chain and the localized band of the spin-$\downarrow$ chain (or vice versa) through spin-flip couplings, leading to a critical phase with mobility edges. In other words, the non-Abelian interchain couplings split the two initially merged critical points of two decoupled chains and move them along opposite directions in the parameter space. The final result is the expansion of critical points of two originally disconnected chains to a critical phase of the non-Abelian coupled chain. Such a mechanism of generating critical phases may not be restricted to systems with non-Abelian potentials. It may also be used to understand the origin of critical phases in 1D systems with sublattice degrees of freedom or long-range hoppings. Nevertheless, regarding the interest of engineering non-Abelian potentials in different physical setups, our discoveries may provide further
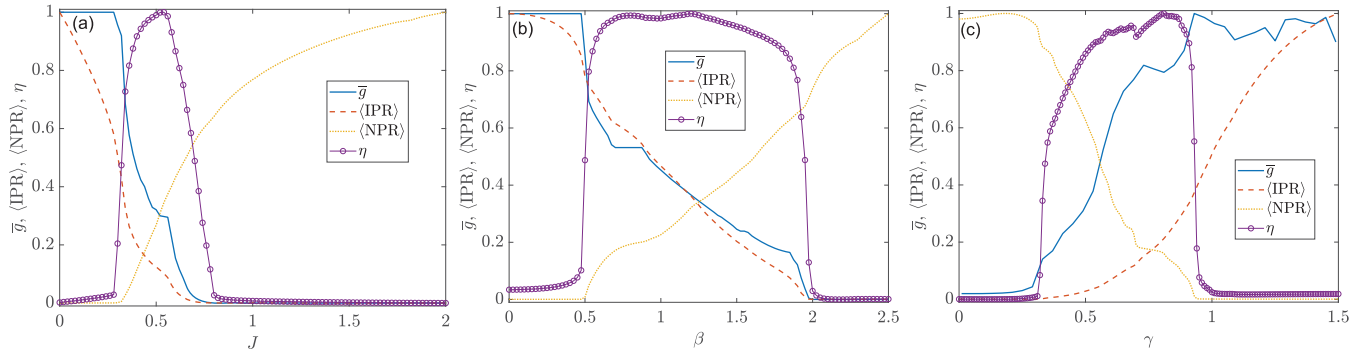
FIG. 13. The averages of AGRs versus system parameters for Models 1, 2, and 3 in panels (a), (b), and (c), respectively. Other system parameters are $(V, \phi) = (1, \pi/10)$ for panel (a), $(J, V, \phi) = (1, 6, \pi/2)$ for panel (b), and $(J, V, \phi) = (1, 0.5, \pi/2)$ for panel (c). We choose $\alpha = (\sqrt{5} - 1)/2$ and $L = 4181$ for all panels. The averages of IPRs, NPRs, and the function η [Eq. (15)] are also plotted to give a better illustration [92].

motivations for the realization of non-Abelian effects in systems beyond clean and Hermitian limits.

To the best of our knowledge, the $\mathcal{PT}$-breaking, localization and topological transitions have not been simultaneously explored in non-Abelian NHQCs. Our work thus introduced typical models and provided initial impetus along this line of study. It also has great experimental relevance regarding the recent realizations of NHQCs [40,41]. In experiments, NHQCs were realized by nonunitary quantum walks in photonic systems [40,41]. Since an artificial spin-1/2 degree of freedom is intrinsically present in the discrete time quantum walk, the existing setups offer natural platforms to explore the critical phases, $\mathcal{PT}$-breaking transitions and localization transitions in non-Abelian NHQCs. The $\mathcal{PT}$-breaking transition may be revealed by measuring the overall energy growth [40] or the overall corrected probability [41] for an initially localized wave packet in nonunitary quantum walks. Both quantities will stay around their initial values in the $\mathcal{PT}$-invariant phase and grow over time in the $\mathcal{PT}$-broken phase. The localization-delocalization transition may be identified from the second moment of an initially localized wave packet [40], which will show a monotonic increase (a low and bounded value) over time in the extended (localized) phase. The critical phase may be further located by measuring both the dynamical IPR and NPR for a localized initial state [41]. Both quantities will deviate clearly from zero in the critical phase. Finally, a direct measurement of the winding number could not be achieved in existing experimental setups. An indirect evidence for the winding number may be provided by the wave localization at a topological interface between two distinct phases [40]. For example, one may spatially connect a half-chain in the extended phase with another half-chain in the localized phase at an interface site j_0. A localized initial state in the extended half-chain will stop spreading and be trapped around j_0 when it reached the interface during the propagation. For Models 1 and 2, the chiral transport of wave packets and non-Hermitian skin effects (NHSEs) may provide further evidences for nontrivial winding numbers [41]. In Model 3, the hopping amplitudes are symmetric and no NHSEs are found, even though there are spectral loops on the complex plane in the critical and localized phases (see Fig. 10). In this case, we could not associate nontrivial winding numbers of the spectrum with NHSEs

and chiral propagations of wave packets. More efforts are required to identify the direct and generic connection between the winding numbers and physical observables in non-Abelian NHQCs.

In future work, it is interesting to explore NHQCs with other types of non-Abelian effects, in superconducting systems, in quasi-one dimension [88] or higher spatial dimensions and under time-periodic drivings [89]. Non-Hermitian localizations and mobility edges were also found in systems with random disorder [90,91]. Meanwhile, in similar models with correlated disorder, the critical phase might be reduced to a critical point. The connection between the realness of an eigenenergy and the localization nature of the related eigenstate could also be different under random and correlated disorders [9,10]. It would thus be interesting to further consider the impact of non-Abelian potentials on the spectrum, localization, topological and entanglement transitions in randomly disordered systems. Beyond the single-particle case, possible many-body localizations and critical phases originated from the competition between non-Abelian quasiperiodic potentials and non-Hermitian effects also deserve to be explored in detail.

APPENDIX: LEVEL STATISTICS

In this Appendix, we discuss one type of tools based on the statistics of energy levels, which may provide further signals about the phases with different localization nature in our non-Abelian NHQCs. Let us denote the normalized right eigenvectors of H [Eq. (2)] and its eigenenergies as $\{|\psi_j\rangle | j = 1, ..., N\}$ and $\{E_j | j = 1, ..., N\}$, with N being the total number of energy levels. Along the real axis, the spacing between the jth and the $(j - 1)$th levels is given by $\epsilon_j = \mathrm{Re} E_j - \mathrm{Re} E_{j-1}$, from which we find the ratio between two adjacent spacings of energy levels as $g_j = \min(\epsilon_j, \epsilon_{j+1})/\max(\epsilon_j, \epsilon_{j+1})$ for $j =$

2, ..., $N - 1$. Here the $\max(\epsilon_j, \epsilon_{j+1})$ and $\min(\epsilon_j, \epsilon_{j+1})$ yield the maximum and minimum between ϵ_j and ϵ_{j+1}. The statistical property of adjacent gap ratios (AGRs) can be obtained by averaging over all g_j in the thermodynamic limit, i.e.,

$$\overline{g} = \lim_{N \to \infty} \frac{1}{N} \sum_j g_j. \tag{A1}$$

We will have $\overline{g} \to 0$ if all the bulk eigenstates are extended. Comparatively, we expect $\overline{g}$ to approach a constant $\overline{g}_{\max} > 0$ if all the bulk eigenstates are localized. If $\overline{g} \in (0, \overline{g}_{\max})$, extended and localized eigenstates should coexist and the system should be in a critical phase. The $\overline{g}$ may thus be utilized to distinguish phases with different localization nature in 1D non-Hermitian systems [35].

In Fig. 13, we report the averages of AGRs $\overline{g}$ for our three non-Abelian NHQC models in some typical situations. For Models 1 and 2, we observe that the $\overline{g}$ indeed approaches zero and a finite constant $\overline{g}_{\max}$ in the extended and localized phases, respectively, and varying between them in the critical phase. For Model 3, we also observe different tendencies for $\overline{g}$ in different phases. However, the $\overline{g}$ of Model 3 shows some oscillations in the localized phase, which indicate that the level statistics may have more complicated structures when the non-Abelian potential is also non-Hermitian.

[1] S. Aubry and G. André, Ann. Israel Phys. Soc. **3**, 133 (1980).

[2] P. G. Harper, Single band motion of conduction electrons in a uniform magnetic field, Proc. Phys. Soc. London, Sect. A **68**, 874 (1955).

[3] J. B. Sokoloff, Unusual band structure, wave function, and electrical conductance in crystals with incommensurate periodic potentials, Phys. Rep. **126**, 189 (1985).

[4] B. Kramer and A. MacKinnon, Localization: Theory and experiment, Rep. Prog. Phys. **56**, 1469 (1993).

[5] A. Jagannathan, The Fibonacci quasicrystal: Case study of hidden dimensions and multifractality, Rev. Mod. Phys. **93**, 045001 (2021).

[6] P. Sarnak, Spectral behavior of quasi periodic potentials, Commun. Math. Phys. **84**, 377 (1982).

[7] A. Jazaeri and I. I. Satija, Localization transition in incommensurate non-Hermitian systems, Phys. Rev. E **63**, 036222 (2001).

[8] Q. Zeng, S. Chen, and R. Lü, Anderson localization in the non-Hermitian Aubry-André-Harper model with physical gain and loss, Phys. Rev. A **95**, 062118 (2017).

[9] H. Jiang, L. Lang, C. Yang, S. Zhu, and S. Chen, Interplay of non-Hermitian skin effects and Anderson localization in nonreciprocal quasiperiodic lattices, Phys. Rev. B **100**, 054301 (2019).

[10] S. Longhi, Topological Phase Transition in Non-Hermitian Quasicrystals, Phys. Rev. Lett. **122**, 237601 (2019).

[11] S. Longhi, Metal-insulator phase transition in a non-Hermitian Aubry-André-Harper model, Phys. Rev. B **100**, 125157 (2019).

[12] T. Liu, H. Guo, Y. Pu, and S. Longhi, Generalized Aubry-André self-duality and mobility edges in non-Hermitian quasiperiodic lattices, Phys. Rev. B **102**, 024205 (2020).

[13] Y. Liu, X.-P. Jiang, J. Cao, and S. Chen, Non-Hermitian mobility edges in one-dimensional quasicrystals with parity-time symmetry, Phys. Rev. B **101**, 174205 (2020).

[14] Q. Zeng, Y. Yang, and R. Lü, Topological phases in one-dimensional nonreciprocal superlattices, Phys. Rev. B **101**, 125418 (2020).

[15] Q. Zeng, Y. Yang, and Y. Xu, Topological phases in non-Hermitian Aubry-André-Harper models, Phys. Rev. B **101**, 020201(R) (2020).

[16] L. Zhai, S. Yin, and G. Huang, Many-body localization in a non-Hermitian quasiperiodic system, Phys. Rev. B **102**, 064206 (2020).

[17] Q. Zeng and Y. Xu, Winding numbers and generalized mobility edges in non-Hermitian systems, Phys. Rev. Res. **2**, 033052 (2020).

[18] S. Longhi, Phase transitions in a non-Hermitian Aubry-André-Harper model, Phys. Rev. B **103**, 054203 (2021).

[19] Y. Liu, Y. Wang, Z. Zheng, and S. Chen, Exact non-Hermitian mobility edges in one-dimensional quasicrystal lattice with exponentially decaying hopping and its dual lattice, Phys. Rev. B **103**, 134208 (2021).

[20] Y. Liu, Y. Wang, X. Liu, Q. Zhou, and S. Chen, Exact mobility edges, $\mathcal{PT}$-symmetry breaking, and skin effect in one-dimensional non-Hermitian quasicrystals, Phys. Rev. B **103**, 014203 (2021).

[21] Z. Xu and S. Chen, Dynamical evolution in a one-dimensional incommensurate lattice with $\mathcal{PT}$ symmetry, Phys. Rev. A **103**, 043325 (2021).

[22] X. Cai, Boundary-dependent self-dualities, winding numbers, and asymmetrical localization in non-Hermitian aperiodic one-dimensional models, Phys. Rev. B **103**, 014201 (2021).

[23] L. Tang, G. Zhang, L. Zhang, and D. Zhang, Localization and topological transitions in non-Hermitian quasiperiodic lattices, Phys. Rev. A **103**, 033325 (2021).

[24] T. Liu, S. Cheng, H. Guo, and X. Gao, Fate of Majorana zero modes, exact location of critical states, and unconventional real-complex transition in non-Hermitian quasiperiodic lattices, Phys. Rev. B **103**, 104203 (2021).

[25] L. Zhai, G. Huang, and S. Yin, Cascade of the delocalization transition in a non-Hermitian interpolating Aubry-André-Fibonacci chain, Phys. Rev. B **104**, 014202 (2021).

[26] L. Zhou, Floquet engineering of topological localization transitions and mobility edges in one-dimensional non-Hermitian quasicrystals, Phys. Rev. Res. **3**, 033184 (2021).

[27] L. Zhou and W. Han, Non-Hermitian quasicrystal in dimerized lattices, Chin. Phys. B **30**, 100308 (2021).

[28] Z.-H. Wang, F. Xu, L. Li, D. Xu, and B. Wang, Unconventional real-complex spectral transition and Majorana zero modes in nonreciprocal quasicrystals, Phys. Rev. B **104**, 174501 (2021).

[29] Y. Liu, Q. Zhou, and S. Chen, Localization transition, spectrum structure, and winding numbers for one-dimensional non-Hermitian quasicrystals, Phys. Rev. B **104**, 024201 (2021).

[30] X. Cai, Localization and topological phase transitions in non-Hermitian Aubry-André-Harper models with p-wave pairing, Phys. Rev. B **103**, 214202 (2021).

[31] S. Longhi, Non-Hermitian Maryland model, Phys. Rev. B **103**, 224206 (2021).

[32] A. P. Acharya, A. Chakrabarty, and D. K. Sahu, Localization, $\mathcal{PT}$-symmetry breaking and topological transitions in non-Hermitian quasicrystals, Phys. Rev. B **105**, 014202 (2022).

[33] C. Yuce and H. Ramezani, Coexistence of extended and localized states in the one-dimensional non-Hermitian Anderson model, Phys. Rev. B **106**, 024202 (2022).

[34] L. Zhou and Y. Gu, Topological delocalization transitions and mobility edges in the nonreciprocal Maryland model, J. Phys.: Condens. Matter **34**, 115402 (2022).

[35] W. Han and L. Zhou, Dimerization-induced mobility edges and multiple reentrant localization transitions in non-Hermitian quasicrystals, Phys. Rev. B **105**, 054204 (2022).

[36] L. Zhou and W. Han, Driving-induced multiple $\mathcal{PT}$-symmetry breaking transitions and reentrant localization transitions in non-Hermitian Floquet quasicrystals, Phys. Rev. B **106**, 054307 (2022).

[37] X. Xia, K. Huang, S. Wang, and X. Li, Exact mobility edges in the non-Hermitian t_1-t_2 model: Theory and possible experimental realizations, Phys. Rev. B **105**, 014207 (2022).

[38] T. Liu and X. Xia, Real-complex transition driven by quasiperiodicity: A class of non-$\mathcal{PT}$ symmetric models, Phys. Rev. B **105**, 054201 (2022).

[39] L. Zhai, G. Huang, and S. Yin, Nonequilibrium dynamics of the localization-delocalization transition in the non-Hermitian Aubry-André model, Phys. Rev. B **106**, 014204 (2022).

[40] S. Weidemann, M. Kremer, S. Longhi and A. Szameit, Topological triple phase transition in non-Hermitian Floquet quasicrystals, Nature (London) **601**, 354 (2022).

[41] Q. Lin, T. Li, L. Xiao, K. Wang, W. Yi, and P. Xue, Topological Phase Transitions And Mobility Edges in Non-Hermitian Quasicrystals, Phys. Rev. Lett. **129**, 113601 (2022).

[42] S. Longhi, Non-Hermitian topological mobility edges and transport in photonic quantum walks, Opt. Lett. **47**, 2951 (2022).

[43] X. Cai, Localization transitions and winding numbers for non-Hermitian Aubry-André-Harper models with off-diagonal modulations, Phys. Rev. B **106**, 214207 (2022).

[44] W. Chen, S. Cheng, J. Lin, R. Asgari, and X. Gao, Breakdown of the correspondence between the real-complex and delocalization-localization transitions in non-Hermitian quasicrystals, Phys. Rev. B **106**, 144208 (2022).

[45] L.-M. Chen, Y. Zhou, S. A. Chen, and P. Ye, Quantum entanglement of non-Hermitian quasicrystals, Phys. Rev. B **105**, L121115 (2022).

[46] J. Dalibard, F. Gerbier, G. Juzeliūnas, and P. Öhberg, Colloquium: Artificial gauge potentials for neutral atoms, Rev. Mod. Phys. **83**, 1523 (2011).

[47] M. Lewenstein, A. Sanpera, and V. Ahufinger, *Ultracold Atoms in Optical Lattices* (Oxford University Press, Oxford, UK, 2012).

[48] U.-J. Wiese, Ultracold quantum gases and lattice systems: Quantum simulation of lattice gauge theories, Ann. Phys. **525**, 777 (2013).

[49] N. Goldman, G. Juzeliūnas, P. Öhberg, and I. B. Spielman, Light-induced gauge fields for ultracold atoms, Rep. Prog. Phys. **77**, 126401 (2014).

[50] N. Goldman, J. C. Budich, and P. Zoller, Topological quantum matter with ultracold gases in optical lattices, Nat. Phys. **12**, 639 (2016).

[51] M. Aidelsburger, S. Nascimbene, and N. Goldman, Artificial gauge fields in materials and engineered systems, C. R. Phys. **19**, 394 (2018).

[52] Y. Han, W. Yi, and W. Zhang, *Physics on Ultracold Quantum Gases* (World Scientific Press, Singapore, 2019).

[53] H. Zhai, *Ultracold Atomic Physics* (Cambridge University Press, Cambridge, UK, 2021).

[54] D. Hofstadter, Energy levels and wave functions of Bloch electrons in rational and irrational magnetic fields, Phys. Rev. B **14**, 2239 (1976).

[55] K. Osterloh, M. Baig, L. Santos, P. Zoller, and M. Lewenstein, Cold Atoms in Non-Abelian Gauge Potentials: From The Hofstadter "moth" to Lattice Gauge Theory, Phys. Rev. Lett. **95**, 010403 (2005).

[56] I. I. Satija, D. C. Dakin, and C. W. Clark, Metal-Insulator Transition Revisited for Cold Atoms in Non-Abelian Gauge Potentials, Phys. Rev. Lett. **97**, 216401 (2006).

[57] I. I. Satija, D. C. Dakin, J. Y. Vaishnav, and C. W. Clark, Physics of a two-dimensional electron gas with cold atoms in non-Abelian gauge potentials, Phys. Rev. A **77**, 043410 (2008).

[58] J. Wang and J. Gong, Butterfly Floquet Spectrum in Driven SU(2) Systems, Phys. Rev. Lett. **102**, 244102 (2009).

[59] N. Goldman, A. Kubasiak, P. Gaspard, and M. Lewenstein, Ultracold atomic gases in non-Abelian gauge potentials: The case of constant Wilson loop, Phys. Rev. A **79**, 023624 (2009).

[60] N. Goldman, I. Satija, P. Nikolic, A. Bermudez, M. A. Martin-Delgado, M. Lewenstein, and I. B. Spielman, Realistic Time-Reversal Invariant Topological Insulators with Neutral Atoms, Phys. Rev. Lett. **105**, 255302 (2010).

[61] A. Kosior and K. Sacha, Simulation of non-Abelian lattice gauge fields with a single-component gas, Europhys. Lett. **107**, 26006 (2014).

[62] Y. Li, Time-reversal invariant SU(2) Hofstadter problem in three-dimensional lattices, Phys. Rev. B **91**, 195133 (2015).

[63] J.-Q. Cai, Q.-Y. Yang, Z.-Y. Xue, M. Gong, G.-C. Guo, and Y. Hu, Interplay between non-Hermiticity and non-Abelian gauge potential in topological photonics, arXiv:1812.02610.

[64] Y. Yang, C. Peng, D. Zhu, H. Buljan, J. D. Joannopoulos, B. Zhen, and M. Soljačić, Synthesis and observation of non-Abelian gauge fields in real space, Science **365**, 1021 (2019).

[65] E. G. Guan, H. Yu, and G. Wang, Non-Abelian gauge potentials driven localization transition in quasiperiodic optical lattices, Phys. Lett. A **384**, 126152 (2020).

[66] Y. Yang, B. Zhen, J. D. Joannopoulos, and M. Soljačić, Non-Abelian generalizations of the Hofstadter model: Spin-orbit-coupled butterfly pairs, Light: Sci. Appl. **9**, 177 (2020).

[67] V. Liu, Y. Yang, J. D. Joannopoulos, and M. Soljačić, Three-dimensional non-Abelian generalizations of the Hofstadter model: Spin-orbit-coupled butterfly trios, Phys. Rev. B **104**, 115127 (2021).

[68] D. Cheng, K. Wang, and S. Fan, Artificial Non-Abelian Lattice Gauge Fields for Photons in The Synthetic Frequency Dimension, Phys. Rev. Lett. **130**, 083601 (2023).

[69] S. M. Girvin and K. Yang, *Modern Condensed Matter Physics* (Cambridge University Press, Cambridge, UK, 2019).

[70] S. Roy, T. Mishra, B. Tanatar, and S. Basu, Reentrant Localization Transition in a Quasiperiodic Chain, Phys. Rev. Lett. **126**, 106803 (2021).

[71] L. Zhou, Entanglement spectrum and entropy in Floquet topological matter, Phys. Rev. Res. **4**, 043164 (2022).

[72] I. Peschel, Calculation of reduced density matrices from correlation functions, J. Phys. A: Math. Gen. **36**, L205 (2003).

[73] L. Herviou, J. H. Bardarson, and N. Regnault, Defining a bulk-edge correspondence for non-Hermitian Hamiltonians via singular-value decomposition, Phys. Rev. A **99**, 052118 (2019).

[74] L. Herviou, N. Regnault, and J. H. Bardarson, Entanglement spectrum and symmetries in non-Hermitian fermionic non-interacting models, SciPost Phys. **7**, 069 (2019).

[75] P.-Y. Chang, J.-S. You, X. Wen, and S. Ryu, Entanglement spectrum and entropy in topological non-Hermitian systems and nonunitary conformal field theory, Phys. Rev. Res. **2**, 033069 (2020).

[76] S. Mu, C. H. Lee, L. Li, and J. Gong, Emergent Fermi surface in a many-body non-Hermitian fermionic chain, Phys. Rev. B **102**, 081115(R) (2020).

[77] L.-M. Chen, S. A. Chen, and P. Ye, Entanglement, non-Hermiticity, and duality, SciPost Phys. **11**, 003 (2021).

[78] Y.-B. Guo, Y.-C. Yu, R.-Z. Huang, L.-P. Yang, R.-Z. Chi, H.- J. Liao, and T. Xiang, Entanglement entropy of non-Hermitian free fermions, J. Phys.: Condens. Matter **33**, 475502 (2021).

[79] N. Okuma and M. Sato, Quantum anomaly, non-Hermitian skin effects, and entanglement entropy in open systems, Phys. Rev. B **103**, 085428 (2021).

[80] C. Ortega-Taberner. L. Rødland, and M. Hermanns, Polarization and entanglement spectrum in non-Hermitian systems, Phys. Rev. B **105**, 075103 (2022).

[81] We rescaled some quantities in order for a more compact illustration. The presented $E_I^{\max}$ is rescaled by its maximum over the considered domain of system parameters in the figure. The presented η is shifted and rescaled as $[\eta - \min(\eta)]/\max[\eta - \min(\eta)]$, where the $\min(\eta)$ and $\max(\eta)$ refer to the minimum and maximum of η over the considered domain of system parameters in the figure. Both the values of the presented $E_I^{\max}$ and η are thus confined in the range [0, 1].

[82] I. Y. Goldsheid and B. A. Khoruzhenko, Distribution of Eigenvalues in Non-Hermitian Anderson Models, Phys. Rev. Lett. **80**, 2897 (1998).

[83] J. T. Chalker and B. Mehlig, Eigenvector Statistics in Non-Hermitian Random Matrix Ensembles, Phys. Rev. Lett. **81**, 3367 (1998).

[84] L. G. Molinari, Non-Hermitian spectra and Anderson localization, J. Phys. A: Math. Theor. **42**, 265204 (2009).

[85] R. Hamazaki, K. Kawabata, N. Kura, and M. Ueda, Universality classes of non-Hermitian random matrices, Phys. Rev. Res. **2**, 023286 (2020).

[86] L. Sá, P. Ribeiro, and T. Prosen, Complex Spacing Ratios: A Signature of Dissipative Quantum Chaos, Phys. Rev. X **10**, 021019 (2020).

[87] S. Ghosh, S. Gupta, and M. Kulkarni, Spectral properties of disordered interacting non-Hermitian systems, Phys. Rev. B **106**, 134202 (2022).

[88] S. Mu, L. Zhou, L. Li, and J. Gong, Non-Hermitian pseudo mobility edge in a coupled chain system, Phys. Rev. B **105**, 205402 (2022).

[89] L. Zhou and J. Gong, Non-Hermitian Floquet topological phases with arbitrarily many real-quasienergy edge states, Phys. Rev. B **98**, 205417 (2018).

[90] N. Hatano and D. R. Nelson, Localization Transitions in Non-Hermitian Quantum Mechanics, Phys. Rev. Lett. **77**, 570 (1996).

[91] J. Feinberg and A. Zee, Non-Hermitian localization and delocalization, Phys. Rev. E **59**, 6433 (1999).

[92] We have scaled all the quantities to restrict their ranges to [0, 1] (see also Ref. [81]). The $\bar{g}$, $\langle IPR \rangle$ and $\langle NPR \rangle$ are scaled by the maximum of AGRs, IPRs, and NPRs at each J, β, and γ for the three models. The nonscaled values of $\bar{g}$ are approximately 0.44, 0.49, and 0.41 for Models 1, 2, and 3 in their localized phases.